Article

CO Oxidation on a CeO/Pt(111) Inverse Model Catalyst Surface: Catalytic Promotion and Tuning of Kinetic Phase Diagrams

Y. Suchorski, R. Wrobel, S. Becker, and H. Weiss

J. Phys. Chem. C, **2008**, 112 (50), 20012-20017 • Publication Date (Web): 19 November 2008

CO Oxidation on a CeO_x/Pt(111) Inverse Model Catalyst Surface: Catalytic Promotion and Tuning of Kinetic Phase Diagrams

Y. Suchorski,*,† R. Wrobel,§,‡ S. Becker,‡ and H. Weiss‡

Institute of Materials Chemistry, Vienna University of Technology, Veterinärplatz 1, A-1210 Vienna, Austria and Chemisches Institut, Otto-von-Guericke-Universität Magdeburg, Universitätsplatz 2, D-39106 Magdeburg, Germany

Received: July 8, 2008

Nanosized 2D ceria islands randomly distributed over the Pt(111) surface have been prepared by oxidation of the nucleating Ce submonolayer and characterized using XPS and STM for coverages of 0.3 and 0.7 ML. Catalytic CO oxidation over the resulting, well-defined CeO_x/Pt(111) model catalytic system of the "inverse supported catalyst" type has been studied using the UHV chamber as a flow reactor. The CO_2 production rate was monitored mass spectrometrically in the temperature range of 413 to 553 K at variable CO/O_2 compositions in the 10^{-5} mbar pressure range. The behavior of the present CeO_x/Pt(111) system in the CO oxidation reaction is summarized in kinetic phase diagrams separating regions of high and low reactivity (both monostable) and that of bistability. A significantly enhanced reactivity and a remarkable shift of the bistable region of the reaction toward higher CO pressures were observed when compared to a clean Pt(111) surface. An "active border" concept is proposed to explain the strong local enhancement of catalytic activity.

Introduction

A significant percentage of modern heterogeneous catalysts used in environmental or industrial applications consists of metal particles supported by oxides.[1] Since the kinetics of surface reactions in such dispersed systems may markedly deviate from the kinetics of corresponding reactions on single crystal surfaces, model systems which mimic the properties of real catalysts are required and have been designed in many variations.[2−4] An important model type is composed of a single crystal metal surface covered by small oxide islands. This type of model catalysts is called "inverse model catalysts" due to a complementary character of these systems relatively to the traditional models consisting of metals dispersed on oxide supports and to the commercial oxide-supported catalysts.[5,6] The possibility of varying the oxide coverage from the rarefied submonolayer to dense multilayer films in a microscopically controlled way (e.g., by using the STM for characterization of the oxide formation[7−9]) allows study of the role of the metal-oxide boundaries in such systems.[9,10] In addition, the "inverse model catalysts" are particularly suited as test systems for Monte Carlo (MC) model studies of the supported metal catalysts. From the experimental point of view, the possibility of using the well-established preparation techniques for single crystal surfaces and the accessibility of the conducting metal surfaces to the full spectrum of surface analytics makes such systems beneficial model objects.

In general, model systems are fabricated for studying surface reactions of practical relevance such as the environmentally important catalytic CO oxidation in order to bridge, e.g., the materials gap. In choosing the catalytic surface (usually a well-defined platinum metal crystal) that shall serve as basis for the inverse catalyst model system, one has to consider a variety of complex nonequilibrium phenomena such as bistability, self-sustained spatiotemporal oscillations, and chaotic behavior which occur on the differently oriented platinum metal surfaces usually used for practical CO conversion. A great amount of experimental and theoretical work has been done aimed at the understanding of the experimentally observed dynamical phenomena.[11−13]

The CO + O/Pt(111) system is a certain exception among the CO + O/Pt(hkl) reaction systems since it does not exhibit spatiotemporal oscillations as usually observed on the "open" Pt planes under UHV conditions. On the macroscopic scale, two stable steady states are observed for this system, a *low-reactivity* state with a predominantly CO covered surface and a *high-reactivity* state corresponding to the oxygen-covered surface. Variation of external control parameters causes kinetic transitions between these two states and in the case the parameters are varied cyclewise a hysteresis is observed manifesting the existence of a region of *bistability*.[14] Due to the relative simplicity of this system, it is well studied both experimentally [11,14−16] and theoretically, where the mean field theory based on nonlinear partial differential equations resulting from the consideration of the Langmuir−Hinshelwood mechanism[17] as well as the MC approach [18,19] were applied (see also a comprehensive review[20] and references therein). All this makes the Pt(111) surface to a suitable candidate for an "inverse model catalyst".

Recently, well defined model systems of the "inverse" type consisting of ceria nanoformations on Rh(111),[8] Pt(111),[9] and Cu(111)[21] surfaces were created. Two of them, based on the Rh(111) and Pt(111) surfaces were subjected to the CO oxidation reaction in which the titration of the oxygen-precovered CeO_x/Rh(111) surface with CO[8] and an in situ XPS- and MS-study of the reaction on CeO_x/Pt(111) using the UHV chambers as flow reactors[9] were performed. In the latter study, an enhanced reactivity of the CeO_x/Pt(111) system and a remarkable shift of the bistable region of the reaction toward higher CO pressures when compared to a clean Pt(111) surface

* To whom correspondence should be addressed. Tel: +43-1-250773816. E-mail: yuri.suchorski@imc.tuwien.ac.at.
† Institute of Materials Chemistry, Vienna University of Technology.
‡ Chemisches Institut, Otto-von-Guericke-Universität Magdeburg.
§ On leave from Technical University of Szczecin, Szczecin, Poland

10.1021/jp806033v CCC: $40.75
Published on Web 11/19/2008

were detected for a submonolayer ceria coverage of $\Theta = 0.3$, and a pronounced redox behavior of the CeO_x formations that follows synchronously the hysteresis cycle of the reaction was observed.

In the present investigation, we continue the approach applied in our previous study,[9] diversifying the ceria submonolayer coverages on Pt(111) surface in order to vary the contribution of the oxide-metal boundary, and extending the external parameters (p_{CO}, p_{O2}, T). The goal is to construct the kinetic phase diagrams for the CO oxidation on the CO_x/Pt(111) model system and to track the ceria-induced effects on the CO oxidation in the CeO_x/Pt(111) inverse catalyst model system.

Experimental Section

The experiments were performed in a multipurpose three-chamber ultrahigh vacuum (UHV) surface analysis system operating at base pressures $\leq 10^{-10}$ mbar. The preparation chamber includes facilities for sample cleaning, Ce-overlayer deposition and the control of surface composition and structure by combined Auger electron spectroscopy and low energy electron diffraction (AES, LEED; *SPECS, ErLEED 150*). In the analysis chambers X-ray photoelectron spectroscopy (XPS; *SPECS, Phoibos-150*) and scanning tunnelling microscopy (STM; *Omicron NanoTechnology, VT-AFM/STM*) are accommodated. During in situ monitoring of the CO oxidation, the differentially pumped UHV chambers were run as constant flow reactors by admitting the reactive gases (CO, O_2) via leak valves from constant pressure reservoirs. The pumping speed was kept constant for all the CO oxidation reaction experiments described here.

The Pt(111) single crystal sample (a 1-mm thick disk of 10 mm in diameter) was mounted on a standard Mo sample plate, and could be cooled to $T < 100$ K as well as heated to $T > 1400$ K (by electron bombardment from the back). The temperature of the crystal was measured with a chromel-alumel thermocouple mechanically contacted to the crystal. The clean Pt(111) surface was prepared by a standard surface cleaning procedure consisting of 1.5 keV argon ion sputtering at room temperature followed by annealing in oxygen (6×10^{-8} mbar) at 750 K and flashing in UHV to 1050 K. After several repetitions of the above procedure no contamination could be detected by XPS and a sharp hexagonal LEED pattern with low background was observed.

Cerium overlayers were deposited using a commercial UHV evaporator (*Focus EFM 3, Omicron NanoTechnology*) with an evaporation rate of 0.25 ML/min calibrated in independent AES experiments for Ce submonolayers on a Cu(111) single crystal surface following the procedure described in ref 22. The XPS spectra (pass energy 10 eV, step size 0.1 − 0.2 eV) were recorded with a 150-mm hemispherical energy analyzer using a Mg Kα (1253.64 eV) X-ray source for excitation. The CO oxidation on the clean Pt(111) single crystal surface and on the CeO_x/Pt(111) system was monitored via the amu = 44 (CO_2) mass spectrometer signal (MS; *MKS Instruments, VacCheck*).

Results and Discussion

The actual interest in ceria−platinum metal model systems originates mainly from the wide use of ceria additives in commercial automotive exhaust catalysts due to their attenuating role as oxygen buffer in the fast gas-composition variations under lean/rich conditions.[23,24] However, despite the increasing interest, atomic-scale model studies of the role of ceria and the ceria/metal interface in the catalytic CO oxidation on platinum metals are rather scarce.[25,26] The main hindrance in the creation of well-defined model systems necessary for such studies is the interfacial Ce−platinum metal alloying starting already around room temperature, which makes the effective separation of coadsorption- and substrate-caused effects difficult.[27,28]

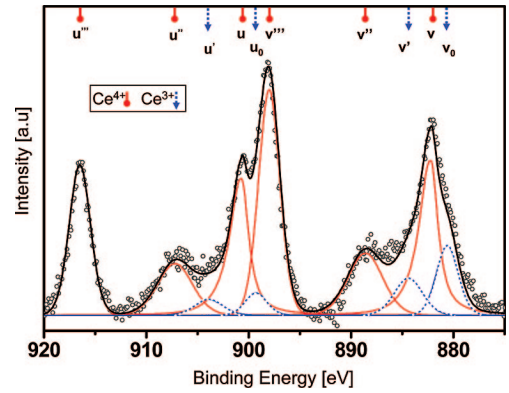

Figure 1. Typical Ce 3d XP spectrum of a CeO_x/Pt(111) inverse model catalyst system prepared by oxidation of a Ce submonolayer ($\Theta = 0.7$ ML) deposited on the Pt(111) surface at 125 K, during warming-up to 300 K in oxygen at $p_{O2} = 1.3 \times 10^{-6}$ mbar. The spectrum deconvolution provides a Ce oxidation state of 3.9.

Depositing Ce in UHV in submonolayer quantities on the Pt(111) surface precooled to 125 K and oxidizing the nucleating Ce islands by admittance of oxygen at 10^{-6} mbar while the sample is successively warmed up to 300 K allowed us to succeed in the creation of an alloy-free CeO_x/Pt(111) model system.[9] In this experimental procedure, oxygen adsorption acts as a kind of stabilizer for the nucleating Ce islands due to immediate CeO_x formation at low temperatures.[28] The resulting model system consisted of dense CeO_x islands (with $x \approx 1.75-1.95$, as confirmed by XPS analysis) of 2−7 nm size more or less uniformly distributed over the Pt(111) surface, as demonstrated by STM.[9] In distinction to our previous contribution,[9] where only a single CeO_x coverage of $\Theta = 0.3$ was realized, and the CO oxidation was studied at a fixed temperature, we increased in the present study the CeO_x coverage to $\Theta = 0.7$, thus achieving a different spatial configuration of our model system. The statistical analysis of the STM pictures provides the same effective mean size of 3.5 nm for ceria islands for both ($\Theta = 0.3$ and $\Theta = 0.7$) coverages. Thus, we could directly compare the catalytic performance of both model systems differing by coverage and by average border length (0.3 and 0.6 nm per nm^2 of Pt surface, corespondingly) at different external parameters.

Figure 1 presents the Ce 3d XP spectrum of a CeO_x/Pt(111) system with $\Theta = 0.7$, with an average Ce oxidation state of ~3.9 in the freshly prepared CeO_x islands as obtained by deconvolution of the Ce 3d peaks. It has to be noted that the increase in the CeO_x coverage from 0.3 to 0.7 significantly facilitated the determination of the Ce oxidation state in the present system due to the increase in the Ce signal intensity in comparison to the experiments in ref 9. However, even for the higher coverage the determination of the Ce oxidation state in 2D CeO_x nanoformations from the XP signal still remains difficult because of presence of two oxidation states (Ce^{3+} and Ce^{4+}) in partially reduced ceria islands. This leads to the appearance of a complicated Ce 3d spectrum with 10 partially overlapping peaks (due to multielectronic processes [29]). This causes the necessity to consider 30 parameters, namely the peak positions, relative peak intensities, and full widths at half-maximum (FWHMs) for each of 10 peaks simultaneously. In the present evaluation, we followed the procedure (including

individual peak positions) described by Schierbaum[30] where the same fwhm values for the doublets were used and a Shirley background was subtracted. Details of the Ce oxidation state determination, which was in the present case based on the correlation of the XPS data to those of reference CeO_x samples with a known oxidation state (CeO_2 powder artificially reduced by Ar^+-sputtering in UHV), are described elsewhere.[31] The obtained deconvolution parameters were successfully proven in a CeO_x/Cu(111) system where a 12-ML thick Ce film (high Ce 3d XP intensity) was gradually oxidized to the ultimate Ce^{4+} state.[21]

The main objective of the present study was to compare the influence of different surface coverages of the CeO_x/Pt(111) submonolayer on the CO oxidation reaction, and to compare it to the bare Pt(111) surface. Our previous studies of the Li- or Dy-promoted CO oxidation in a heterogeneous nanosized catalytic system have shown that summarizing the system behavior in a kinetic phase diagram, where the regions of monostability, bistability, and temporal oscillations are marked for varying external parameters, may help in elucidating the promoting effects.[32,33] The use of the term "phase diagram" for the description of kinetic transitions from, e.g., active to inactive states is justified by the analogy to equilibrium thermodynamics as noticed by Schlögl already in the seventies of the last century:[34−36] the crucial role in both, equilibrium and nonequilibrium phase transitions, play the cooperative phenomena forming, e.g., ordered structures in an equilibrium, and self-organizing dissipative structures in a nonequilibrium situation. The appearance of instabilities, bifurcations or kinetic oscillations, as it is, e.g., the case in the CO oxidation reaction on platinum metal surfaces, is related from this point of view to the appearance of different competitive reactive "phases".[37]

Such phase diagrams appeared to be helpful in revealing and understanding mechanisms of bistability and oscillations for reactions in homogeneous phase such as the Briggs−Rauscher (BR) or Belousov−Zhabotinsky (BZ) oscillating reaction,[38,39] and are applied since more than one decade also to heterogeneous systems such as CO + O_2/Me.[32,37,40,41] Due to their characteristic shape for the CO oxidation reaction on different Pt, Rh, and Pd surfaces, these diagrams are often referred to as *cross-shaped phase diagrams*[40] or (because of the branching at the transition points) as *bifurcation diagrams*.[32] The effect of promoters becomes clearly visible in these diagrams because of the changed adspecies−surface interactions and the resulting alteration of the sticking and the adsorption/desorption kinetics.

To obtain a kinetic phase diagram of a reaction that exhibits bistability, the experimental parameters have to be varied in a cyclic way to reveal the hysteresis behavior. Figure 2 shows two typical hysteresis loops in the CO_2 production rate R_{CO2} during a cyclic variation of the partial pressure p_{CO} of CO, in the CO oxidation on a clean Pt(111) surface which was used as a reference for our CeO_x/Pt(111) model systems. The surface morphology was controlled prior to the reaction by STM (Figure 2a), and the reaction was run under continuous-flow conditions at constant oxygen pressure of 1.3×10^{-5} mbar and isothermally in a temperature range of 413−553 K (the temperature was kept constant for each hysteresis loop track).

We start with low p_{CO} within the (mono-) stable steady state of high reactivity which loses its stability upon approaching the transition point τ_A (Figure 2b), where the corresponding $p_{CO}^{\tau A}$ depends on p_{O2} and T. Similarly, for the reverse scan the steady state of low reactivity becomes instable at τ_B. Thus, at $p_{CO}^{\tau B} < p_{CO} < p_{CO}^{\tau A}$, the system can be in one of the two steady states, depending on the scan direction. A variation of the sample

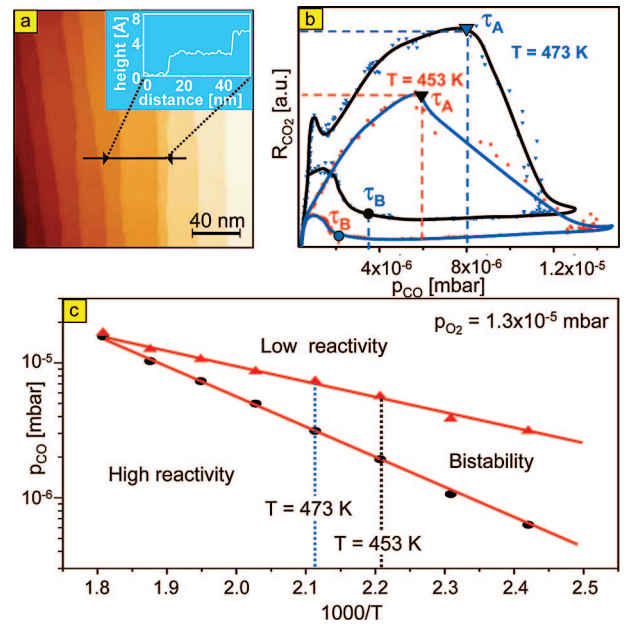

Figure 2. CO oxidation reaction on clean Pt(111) used as reference surface. (a) STM image of clean Pt(111), 200 × 200 nm ($U_{bias} = -0.50$ V, $I = 0.22$ nA). The inset shows a typical atomic step profile. (b) Hysteresis in the CO_2 production rate R_{CO2} as obtained upon cyclic variation of the CO partial pressure for constant oxygen pressure $p_{O2} = 1.3 \times 10^{-5}$ mbar at temperatures of $T = 453$ and 473 K. τ_A and τ_B mark the points at which the kinetic transitions occur. (c) Corresponding kinetic phase diagram. The regions of high reactivity and low reactivity and the region of bistability are denoted. τ_A and τ_B points from (b) at $T = 453$ and 473 K, respectively, are marked.

temperature at constant p_{O2} changes the positions of the transition points τ_A and τ_B as is clearly visible in Figure 2b. Such kinetic transitions are characteristic for a bistable reaction behavior caused by the asymmetric inhibition of the dissociative oxygen adsorption by CO, and are well studied both experimentally[20,32,37,40,41] and theoretically.[42−44] In particular, the pioneering work of Ziff, Gulari, and Barshad[42] should be accentuated because of admitting spatial inhomogeneities usually averaged in mean-field considerations. Studies on microscopically sized surfaces like nanofacets of a Pt field emitter tip[45] or clusters[46] have demonstrated that the bistability remains present, as an inherent property of a monomer−dimer Langmuir−Hinshelwood reaction, also in nanosized reaction systems and is limited only by fluctuation-induced effects.[46−48] These studies have confirmed also the role of the long-range correlations tacitly assumed in the model proposed by Ziff et al.[42]

The series of isothermal hysteresis loops measured for different temperatures in the range 413−533 K are summarized in a phase diagram shown in Figure 2c, where the CO partial pressures corresponding to the τ_A and τ_B points are plotted versus the reciprocal temperature. We note that the hysteresis loops in Figure 2b and the diagram presented in part c are in a good agreement with known results for CO oxidation on Pt(111).[14]

Starting from the clean Pt(111) surface shown in Figure 2a and using the corresponding phase diagram in Figure 2c as a reference, the role of the ceria nanoformations can be studied by a direct comparison: Figure 3a shows the Pt(111) surface with CeO_x islands at $\Theta = 0.3$ ML coverage, and Figure 3b presents two corresponding hysteresis loops obtained at the same external parameters as for the clean Pt(111) surface in Figure 2b. The curves resemble those in Figure 2b but are remarkably shifted to higher CO pressures compared to the clean Pt(111) surface. The corresponding phase diagram for the $CeO_x^{\Theta=0.3}$/

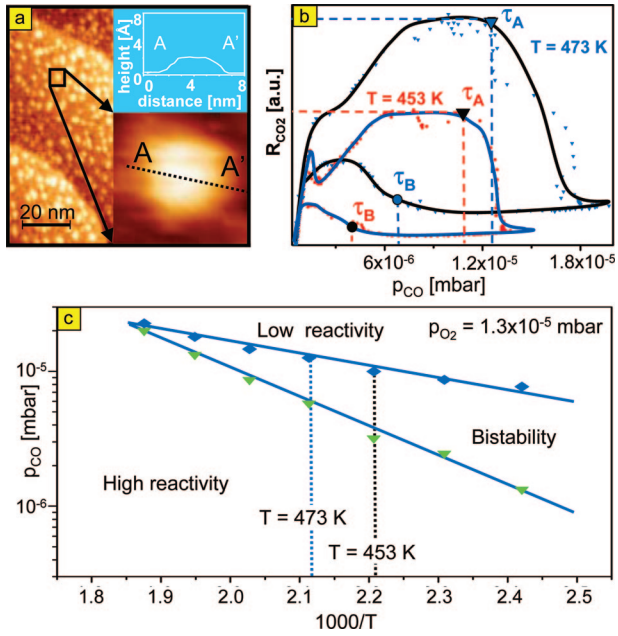

Figure 3. CO oxidation reaction on CeO_x/Pt(111) at $\Theta_{CeOx} = 0.3$. (a) STM image, 100 × 100 nm ($U_{bias} = -0.53$ V, $I = 0.26$ nA). The inset shows a typical CeO_x island profile. (b) Hysteresis in the CO_2 production rate R_{CO2} as obtained upon cyclic variation of the CO partial pressure for constant oxygen pressure $p_{O2} = 1.3 \times 10^{-5}$ mbar and at two constant temperatures $T = 453$ and 473 K. (c) Corresponding kinetic phase diagram. The regions of high reactivity and low reactivity and the region of bistability are denoted. τ_A and τ_B points from (b) at $T = 453$ and 473 K, respectively, are marked.

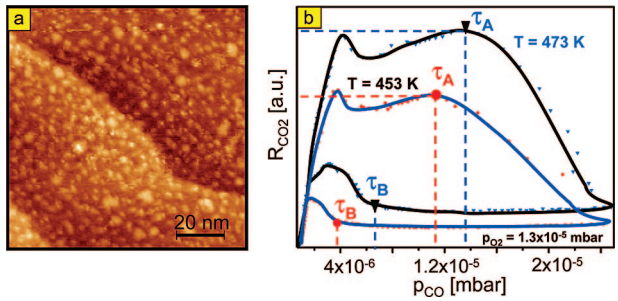

Figure 4. CO oxidation reaction on CeO_x/Pt(111) at $\Theta_{CeOx} = 0.7$. (a) STM image, 100 × 100 nm ($U_{bias} = -0.53$ V, $I = 0.22$ nA). (b) Hysteresis in the CO_2 production rate R_{CO2} as obtained upon cyclic variation of the CO partial pressure for constant oxygen pressure $p_{O2} = 1.3 \times 10^{-5}$ mbar and at two constant temperatures $T = 453$ and 473 K.

Pt(111) model system is accordingly shifted toward higher CO pressures and lower temperatures (see Figure 3c). The catalytic activity (CO_2 production rate) of the Pt(111) surface promoted by ceria increases despite of the evident blocking effect (occupancy of active Pt sites by CeO_x islands). This effect will be discussed in detail below.

Increasing the ceria coverage to 0.7 (Figure 4a) leads to a hardly observable further shift of τ_A and τ_B along the abscissa (Figure 4b) and, correspondingly, of the phase diagram which overlaps within the error bars with that for 0.3 monolayer of ceria (compare Figure 5c). However, an additional moderate increase of the reactivity has been observed, although 70% of the initial catalytically active surface was blocked by CeO_x. For illustration of this effect, hysteresis curves for $\Theta = 0$; 0.3; and 0.7 monolayers of CeO_x scanned at 453 K are summarized in Figure 5a, where the maximal ordinates for individual curves reflect the achievable total catalytic activity of the particular

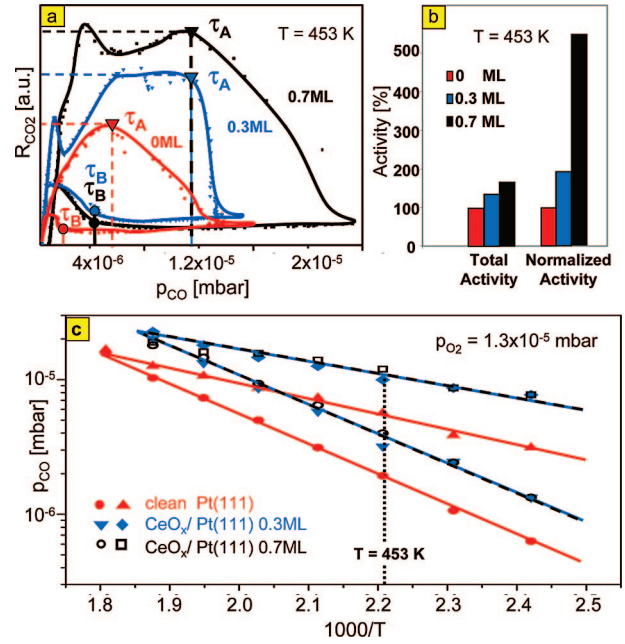

Figure 5. Ceria-induced promoting effects. (a) Comparison of the hysteresis loops obtained for the clean Pt(111) surface and for the $CeO_x^{\Theta=0.3}$/Pt(111) and $CeO_x^{\Theta=0.7}$/Pt(111) systems at $T = 453$ K and $p_{O2} = 1.3 \times 10^{-5}$ mbar. The maximum in the CO_2 production rate R_{CO2} is used as a measure of the catalytic activity of the corresponding system for comparison in (b). (b) Comparison of the catalytic activity of the clean Pt(111), $CeO_x^{\Theta=0.3}$/Pt(111) and $CeO_x^{\Theta=0.7}$/Pt(111) systems toward CO oxidation. Left side bars: total activity; right side bars: activity normalized by the exposed (bare) Pt(111) surface. (c) Kinetic phase diagrams obtained for the clean Pt(111) and for the $CeO_x^{\Theta=0.3}$/Pt(111) and $CeO_x^{\Theta=0.7}$/Pt(111) systems at constant oxygen partial pressure $p_{O2}=1.3 \times 10^{-5}$ mbar. The diagrams for $CeO_x^{\Theta=0.3}$/Pt(111) and for $CeO_x^{\Theta=0.7}$/Pt(111) coincide within the error bars.

systems. The corresponding values are displayed in Figure 5b together with the activity normalized by the exposed Pt(111) surface. The comparison reveals that the CO_2 production per unit of the exposed Pt(111) surface increases for the $CeO_x^{\Theta=0.7}$/Pt(111) system by a factor of more than 5 compared to the nonpromoted Pt(111) surface, and by a factor of about 2.5 relative to the $CeO_x^{\Theta=0.3}$/Pt(111) system. As already mentioned, this increase in activity is not accompanied by an additional noticeable shift or modification of the kinetic phase diagram (Figure 5c).

The explanation for the observed effects can be found in the atomic-scale peculiarities of the spatial electron density distribution at the Pt surface in the vicinity to CeO_x islands (at the Pt−CeO_x interface). Already our earlier experiments with various Pt surfaces predosed with Li and Dy submonolayers have demonstrated that the coadsorption of electropositive adatoms shifts the bistability region in the CO oxidation on Pt toward higher CO pressures.[32,33] This is mainly due to the coadsorbate-induced enhancement of the sticking coefficient of oxygen (see, e.g., ref 49) which can be interpreted as a purely electronic effect caused by the extension of the local electron density farther away from the metal surface.[50] As a result, the precursor potential as well as the dissociation barrier height for molecularly adsorbed species is modified.[51,52] This influences the adsorption/desorption equilibria of CO and molecular O_2 in favor of oxygen. We note, that intentional modification of the electron density distribution near the Pt surface by high electric fields of about 10 V/nm leads to a shift of the bistability region of a similar order of magnitude,[53] supporting thus our present electronic effect consideration.

In the present case, the modified electron density is restricted to a few adsorption sites in the wide area around the CeO_x islands ("active border" region), a rather minor part of the total catalytically active area. This suggests that the additional oxygen supply may originate via spillover from electronically modified regions to the rest of the metal surface and also via diffusion from the CeO_x formations, similar to that suggested for a Pt/CeO_x model catalyst prepared by electron-beam lithography.[54] The pronounced hysteresis-like redox behavior of the oxidation state of Ce in the CeO_x islands during the cyclic variation of p_{CO}, as it was monitored in situ during the ongoing reaction in our recent study,[9] supports this suggestion. An alternative mechanism comprising CO oxidation over the CeO_x surface, as it was detected under ambient pressure conditions,[55] can be rather neglected under the present UHV conditions as was discussed in ref 9 and was proven in our experiments with dense CeO_x films on a Cu(111) substrate.

Apart from enhanced oxygen supply, a certain contribution to the shift of the phase diagram may be related to the altered CO adsorption on the electronically modified Pt surface along the CeO_x/Pt interface. The particular role of the island boundaries in CO adsorption was recently suggested for the ceria/Rh(111) system fabricated by reactive evaporation of Ce on Rh(111).[8] In a study of CO adsorption on a Pt/ceria system consisting of Pt particles dispersed on a ceria film a remarkable decrease in the CO desorption temperature was observed and interpreted as an indication of a significant metal-oxide interaction.[56] The effect was explained by electron transfer from reduced ceria into the Pt d-band which makes Pt more inert toward CO adsorption. Our present results show that the CO/oxygen kinetic equilibrium is influenced for reducing as well as oxidizing conditions to a similar degree, i.e., such electron transfer is rather an inherent property of the CeO_x/Pt interface. This may lead to the existence of a nanosized, partially reduced region of CeO_x along the ceria/Pt border. In the present case of CeO_x nanoformations on Pt(111), small but detectable deviations of x from exactly 2 even under oxidizing conditions were detected, supporting this supposition. In the "reverse" case of Pt particles supported by ceria, such local deviations of the Ce oxidation state might also take place on a nanoscale, but may not yet have been observed because of the averaging of the XPS signal over the macroscopic sample. The nanosized regions along the ceria/Pt border with modified kinetics of CO and oxygen adsorption can play the role of local pace-makers in kinetic transitions from active (oxygen-covered) to inactive (CO-covered) steady states. The transitions seem to start at the interface area spreading then as a wave along the Pt surface, similarly as it was observed on the heterogeneous surface of a Pt field emitter tip where, e.g., the nanosized (331) planes play the role of pace-makers.[53] Laterally resolved techniques like spectroscopic PEEM[57] or MIEEM[58] would help to get an insight into the local spatial distribution of cerium oxidation states on the metal-oxide interface in dispersed systems.

The above reasons for the shift of the phase diagram, especially the enhanced uptake of oxygen, contribute also to the observed ceria promoting effect on the catalytic activity of the present CeO_x/Pt(111) model system. In addition, the enhanced O_2 dissociation rate at the CeO_x/Pt interface may contribute to the reaction rate enhancement, as it is suggested in ref 59. Indeed, the interface step height of ~3Å (see inset in Figure 1) may provide an inhomogeneity which is sufficient to significantly facilitate the O_2 dissociation. Recently, an enhanced CO oxidation rate caused by a noticeable increase of the oxygen dissociation rate on steps of the Pt(411) surface was observed.[60]

The number of modified adsorption sites is related to the island's overall perimeter length and can be modified by varying the CeO_x coverage as has been done, to a certain extent, in the present experiments. Simple geometric considerations that assume a circular shape of the islands and a concentric, one to three adsorption sites wide, electronically modified region around the perimeter area, predict an increase in the number of modified adsorption places by a factor of approximately 5 (referenced to the total unoccupied Pt surface) at increasing CeO_x coverage from $\Theta = 0.3$ to $\Theta = 0.7$. However, the actual catalytic activity improves solely by a factor of about 2.5 (Figure 5b, right-hand diagram). The reason may be that promoted adsorption sites from neighboring islands overlap due to the rather stochastic island distribution, reducing thus the effective "active border" area and the activity enhancement factor. Such a semiquantitative estimation contains, of course, a rather rough average over the inhomogeneously active surface, thus more detailed studies with intermediate and higher CeO_x coverages are required in order to understand the enhancement mechanism.

A possible electronic contribution to the increased reaction rate due to Ce−Pt alloy formation can be excluded: our experiments with an intentionally created Ce−Pt alloy system (via annealing of the Ce submonolayer) have shown a reduced reaction rate in comparison to clean Pt(111) due to the blocking of active sites.

It has also to be noted that the suggested role of an electronically modified area along the metal−oxide interface should not be restricted just to the CO oxidation on platinum group metals: the particle size effects observed in hydrocarbon reactions on oxide-supported metal catalyst,[61] might also be related to the presently discussed local electronic phenomena.

Generally, the CeO_x/Pt systems seem to be promising objects to study the metal−support interaction. The so-called strong metal support interaction (SMSI) observed for Pt particles on titania and ceria is mainly attributed to encapsulation of the metal particles by the oxides.[56,62] In the inverse case of ceria particles on Pt, the corresponding SMSI effect would manifest itself in the immersing of CeO_x particles in the Pt substrate, which however, was not observed in the present study, presumably due to the investigated temperature range of $\leq$723 K (annealing to 800 K and above was necessary to cause the encapsulation in ref 56). Additional STM studies at elevated annealing temperatures are intended to pursue such possible effect.

Conclusions

A well-defined CeO_x/Pt(111) model catalytic system of the "inverse supported catalyst" type consisting of nanosized 2D oxide islands on a Pt(111) surface has been fabricated by oxidation of the nucleating Ce submonolayer for coverages of 0.3 and 0.7 ML. The presence of CeO_x nanoformations has a significant impact on the catalytic performance of the Pt(111) surface in the CO oxidation reaction, inducing a significant shift of the bistability region and thereby of the whole kinetic phase diagram for CO oxidation to higher CO pressures. Despite of the surface blocking effect (by ceria islands) the total catalytic activity increases remarkably, indicating a significant gain of the catalytic activity on the exposed (uncovered) Pt-surface. A concept of an "active border" consisting of an a few adsorption sites wide electronically modified area around the CeO_x islands is proposed to explain the strong local enhancement of catalytic activity.

Acknowledgment. R.W. acknowledges the support by EU Contract HPRN-CT-2002-00191.

References and Notes

(1) Bevy, L. B. *Frontiers in Catalysis Research*; Nova Science Publishers Inc: Hauppauge, NY, 2006.

(2) Freund, H.-J.; Ernst, N.; Bäumer, M.; Rupprechter, G.; Libuda, J.; Kuhlenbeck, H.; Risse T.; Drachsel, W.; Al-Shamery, K.; Hamann, H. In: *Surface Chemistry and Catalysis*; Carley, A. F., Ed.; Kluwer Academic/Plenum Publishers: New York, 2002.

(3) Freund, H.-J. *Surf. Sci.* **2002**, *500*, 271, and references therein.

(4) Avoyan, A.; Rupprechter, G.; Eppler, A. S.; Somorjai, G. A. *Top. Catal.* **2000**, *10*, 107.

(5) Hayek, K.; Fuchs, M.; Klötzer, B.; Reichl, W.; Rupprechter, G. *Top. Catal.* **2000**, *13*, 55.

(6) Leisenberger, F. P.; Surnev, S.; Koller, G.; Ramsey, M. G.; Netzer, F. P. *Surf. Sci.* **2000**, *444*, 211.

(7) Schoiswohl, J.; Surnev, S.; Netzer, F. P. *Top. Catal.* **2005**, *36*, 91, and references therein.

(8) Eck, S.; Castellarin-Cudia, C.; Surnev, S.; Prince, K. C.; Ramsey, M. G.; Netzer, F. P. *Surf. Sci.* **2003**, *536*, 166.

(9) Suchorski, Y.; Wrobel, R.; Becker, S.; Strzelczyk, B.; Drachsel, W.; Weiss, H. *Surf. Sci.* **2007**, *601*, 4843.

(10) Schoiswohl, J.; Eck, S.; Ramsey, M. G.; Andersen, J. N.; Surnev, S.; Netzer, F. P. *Surf. Sci.* **2005**, *580*, 122.

(11) Ertl, G. *Adv. Catal.* **1990**, *37*, 231, and refererences therein.

(12) Schüth, F.; Henry, B. E.; Schmidt, L. D. *Adv. Catal.* **1993**, *39*, 51.

(13) Bykov, V. I.; Elokhin, V. I.; Gorban, A. N.; Yablonskii, G. S. Kinetic Models of Catalytic Reactions. In *Comprehensive Chemical Kinetics*; Elsevier: Amsterdam, 1991; Vol. 32.

(14) Berdau, M.; Yelenin, G G.; Karpowicz, A.; Ehsasi, M.; Christmann, K.; Block, J. H. *J. Chem. Phys.* **1999**, *110*, 11551.

(15) Ehsasi, M.; Matloch, M.; Frank, O.; Block, J. H.; Christmann, K.; Rys, F. S.; Hirschwald, W. *J. Chem. Phys.* **1989**, *91*, 4949.

(16) Gerrard, A. L.; Weaver, J. F. *J. Chem. Phys.* **2005**, *123*, 224703.

(17) Bar, M.; Zülicke, Ch.; Eiswirth, M.; Ertl, G. *J. Chem. Phys.* **1992**, *96*, 8595.

(18) Völkening, S.; Wintterlin, J. *J. Chem. Phys.* **2001**, *114*, 6382.

(19) Petrova, N. V.; Jakovkin, I. N. *Surf. Sci.* **2005**, *578*, 162.

(20) Zhdanov, V. P.; Kasemo, B. *Surf. Sci. Rep.* **2000**, *39*, 25, and references therein.

(21) Wrobel, R.; Suchorski, Y.; Becker, S.; Weiss, H. *Surf. Sci.* **2008**, *602*, 436.

(22) Napetschnig, E.; Schmid, M.; Varga, P. *Surf. Sci.* **2004**, *556*, 1.

(23) Kaspar, J.; Fornasiero, P.; Hickey, N. *Catal. Today* **2003**, *77*, 419.

(24) Di Monte, R.; Kaspar, J. *Top. Catal.* **2004**, *28*, 47.

(25) Tang, J.; Lawrence, J. M.; Hemminger, J. C. *Phys. Rev. B* **1993**, *48*, 15342.

(26) Baddeley, C. J.; Stephenson, A. W.; Hardacre, C.; Tikhov, M.; Lambert, R. M. *Phys. Rev. B* **1997**, *56*, 12589.

(27) Eck, S.; Castellarin-Cudia, C.; Surnev, S.; Ramsey, M. G.; Netzer, F. P. *Surf. Sci.* **2002**, *520*, 173.

(28) Fargues, D.; Gally, A.; Ehrhardt, J. J. *Thin Sol. Films* **1994**, *252*, 105.

(29) Willoud, E.; Delley, B.; Schneider, W. D.; Baer, Y. *Phys. Rev. Lett.* **1984**, *53*, 202.

(30) Schierbaum, K.-D. *Surf. Sci.* **1984**, *399*, 29.

(31) Suchorski, Y.; Gottfriedsen, J.; Wrobel, R.; Strzelczyk, B.; Weiss, H. *Sol. State. Phenom.* **2007**, *128*, 115.

(32) Suchorski, Y.; Imbihl, R.; Medvedev, V. K. *Surf. Sci.* **1998**, *401*, 392.

(33) Losovyj, Y. B.; Ketsman, I. V.; Kostrobij, P. P.; Suchorski, Y. *Vacuum* **2001**, *63*, 277.

(34) Schlögl, F. *Z. Phys.* **1971**, *248*, 446.

(35) Schlögl, F. *Z. Phys.* **1972**, *253*, 147.

(36) Schlögl, F. *Ber. Bunsenges. Phys. Chem.* **1980**, *84*, 351.

(37) Ehsasy, M.; Berdau, M.; Rebitzki, T.; Charle, K.-P.; Christmann, K.; Block, J. H. *J. Chem. Phys.* **1993**, *98*, 9177.

(38) Boissonade, J.; de Kepper, P. *J. Phys. Chem.* **1980**, *84*, 501.

(39) *Oscillations and Travelling Waves in Chemical Systems*; Field, R. J., Burger, M., Eds.; Wiley: New York, 1985.

(40) Berdau, M.; Karpowicz, A.; Yelenin, G. G.; Christmann, K.; Block, J. H. *J. Chem. Phys.* **1997**, *106*, 4291.

(41) Wehner, S.; Baumann, F.; Ruckdeschel, M.; Küppers, J. *J. Chem. Phys.* **2003**, *119*, 6823.

(42) Ziff, R. M.; Gullari, E.; Barshad, Y. *Phys. Rev. Lett.* **1986**, *56*, 2553.

(43) Dickmann, R. *Phys. Rev. A* **1986**, *34*, 4246.

(44) Hua, D.-y.; Shao, S.-j.; Lin, Su. *Phys. Rev. E* **2004**, *69*, 46114.

(45) Gorodetskii, V.; Drachsel, W.; Block, J. H. *Catal. Lett.* **1993**, *19*, 223.

(46) Johánek, V.; Laurin, M.; Grant, A. W.; Kasemo, B.; Henry, C. R.; Libuda, J. *Science* **2004**, *304*, 1639.

(47) Suchorski, Y.; Beben, J.; James, E. W.; Evans, J. W.; Imbihl, R. *Phys. Rev. Lett.* **1999**, *82*, 1907.

(48) Suchorski, Y.; Beben, J.; Imbihl, R.; James, E. W.; Liu, D.-J.; Evans, J. W. *Phys. Rev. B* **2001**, *63*, 165417.

(49) Kiskinowa, M. P. In *Poisoning and Promoting in Catalysis Based on Surface Science Concepts and Experiments*; Delmon, B., Yates, J. T., Eds.; Elsevier: Amsterdam 1992, and references therein.

(50) Feibelman, P. J.; Hamann, D. R. *Surf. Sci.* **1985**, *149*, 48.

(51) Luntz, A. C.; Grimbolt, J.; Fowler, D. E. *Phys. Rev. B* **1989**, *39*, 12903.

(52) Osovskii, V. D.; Ptushinskii, Y. G.; Sukretnyi, V. G.; Chuikov; B.A.; Medvedev, V. K.; Suchorski, Y. *Surf. Sci.* **1997**, *377/379*, 664.

(53) Suchorski, Y.; Drachsel, W. *Top. Catal.* **2007**, *46*, 201, and references therein.

(54) Johansson, S.; Österlund, L.; Kasemo, B. *J. Catal.* **2001**, *201*, 275.

(55) Bunluesin, T.; Putna, E. S.; Gorte, R. J. *Catal. Lett.* **1996**, *41*, 1.

(56) Mullins, D. R.; Zhang, K. Z. *Surf. Sci.* **2002**, *513*, 163.

(57) Locatelli, A.; Aballe, L.; Mentes, T. O.; Kiskinova, M.; Bauer, E. *Surf. Interface Anal.* **2006**, *38*, 1554.

(58) Lilienkamp, G.; Suchorski, Y. *Surf. Interface Anal.* **2006**, *38*, 378.

(59) Johansson, S.; Fridell, E.; Kasemo, B. *J. Catal.* **2001**, *200*, 370.

(60) Lewis, H. D.; Burnett, D. J.; Gabelnick, A. M.; Fischer, D. A.; Gland, J. L. *J. Phys. Chem. B* **2005**, *109*, 21847.

(61) Hayek, K.; Kramer, R.; Paal, Z. *Appl. Catal., A* **1997**, *162*, 1.

(62) Tauster, S. J. *Acc. Chem. Res.* **1987**, *20*, 389.

JP806033V